JACS
JOURNAL OF THE AMERICAN CHEMICAL SOCIETY
pubs.acs.org/JACS
Article

Chemical Design of Spin Frustration to Realize Topological Spin Glasses

Stephanie M. Amtry, Arthur C. Campello, Christopher L. Tong, Danilo S. Puggioni, James M. Rondinelli, Young S. Lee, and Danna E. Freedman*

Cite This: https://doi.org/10.1021/jacs.4c10113
Read Online

ABSTRACT: Patterning spins to generate collective behavior is at the core of condensed matter physics. Physicists develop techniques, including the fabrication of magnetic nanostructures and precision layering of materials specifically to engender frustrated lattices. As chemists, we can access such exotic materials through targeted chemical synthesis and create new lattice types by chemical design. Here, we introduce a new approach to induce magnetic frustration on a modified honeycomb lattice through a competition of alternating antiferromagnetic (AFM) and ferromagnetic (FM) nearest-neighbor interactions. By subtly modulating these two types of interactions through facile synthetic modifications, we created two systems: (1) a topological spin glass and (2) a frustrated spin-canted magnet with low-temperature exchange bias. To design this unconventional magnetic lattice, we used a metal−organic framework (MOF) platform, $Ni_3(pymca)_3X_3$ (NipymcaX where pymca = pyrimidine-2-carboxylato and X = Cl^-, Br^-). We isolated two MOFs, NipymcaCl and NipymcaBr, featuring canted Ni^{2+}-based moments. Despite this similarity, differences in the single-ion anisotropies of the Ni^{2+} spins result in magnetic properties for each material. NipymcaCl is a topological spin glass, while NipymcaBr is a rare frustrated magnet with low-temperature exchange bias. Density functional theory calculations and Monte Carlo simulations on the NipymcaX lattice support the presence of magnetic frustration as a result of alternating AFM and FM interactions. Our calculations enabled us to determine the ground-state spin configuration and the distribution of spin−spin correlations relative to paradigmatic kagomé and triangular lattices. This modified honeycomb lattice is similar to the electronic Kekulé-O phase in graphene and provides a highly tunable platform to realize unconventional spin physics.

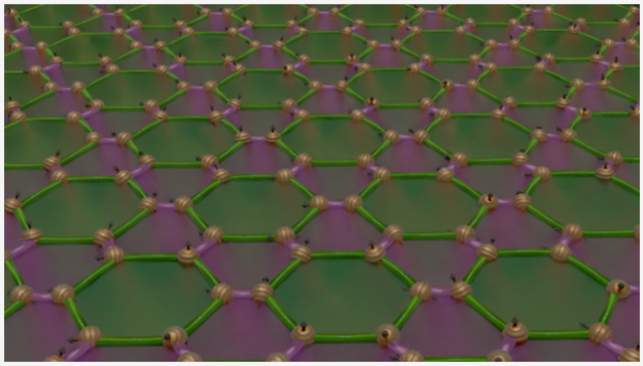

■ INTRODUCTION

Historically, new phenomena in physics have been discovered at the boundaries between phases or by creating electronic structures with instability between potential ground states.[1−5] One can draw an analogy to chemistry, whereby reactivity emerges at phase boundaries, such as in materials transitioning from one allotrope to another. Priming materials for this electronic instability is key to creating new phases of matter, both structurally and electronically. Controlling competing interactions to engender spin frustration is one promising approach to develop these materials.[6−10] The phases that emerge in these materials,[6−11] such as spin liquid states and host exotic states of matter, proposed to enable material technologies such as robust quantum computation[12−14] and unconventional superconductivity.[10,15−17]

Magnetic frustration is essential for engendering a whole host of properties beyond these collective phases. As computational methods emerge for determining the ground state of complex systems,[18−21] a new frontier in dynamics is unfolding. One class of materials with dynamic properties is topological (frustrated) spin glasses. Topological spin glasses manifest frozen, disordered states characterized by magnetic frustration and display unique "memory" and aging dynamics.[22−28] Understanding the dynamic behavior of spin glasses provides fundamental insights into the behavior of complex systems beyond disordered magnets, such as biological neural networks.[29−32] Recently, topological glasses have been found to exhibit exchange bias,[22,23] a phenomenon involving the shifting of a ferromagnet's hysteresis loop due to interactions with a pinning antiferromagnet.[33] This effect has been widely explored in AFM/FM bilayers in nonvolatile magnetic storage technologies.[34−38] Despite this significance, the exact origin of exchange bias remains poorly understood, and controlling and

Received: July 26, 2024
Revised: September 26, 2024
Accepted: September 26, 2024

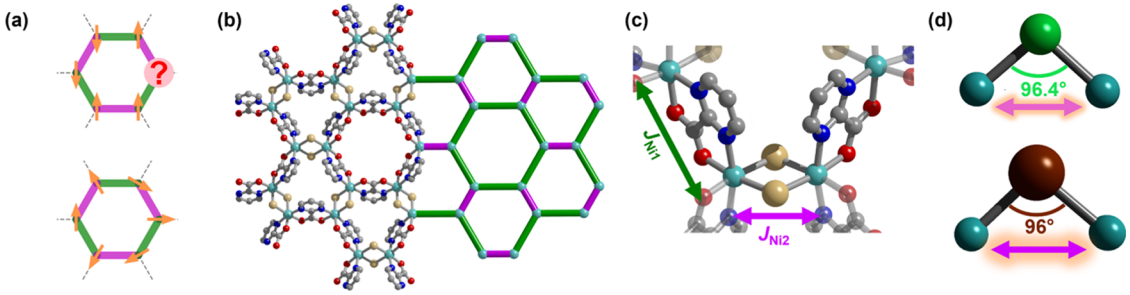

Figure 1. (a) Toy spin diagram of frustration on a honeycomb lattice with alternating AFM and FM nearest-neighbor coupling. (b) Select the crystal structure of a layer of NipymcaX viewed down the crystallographic *ab* plane. The right side stripped away the ligands to provide a schematic of the magnetic honeycomb lattice with alternating AFM (J_{Ni1}, green lines) and FM (J_{Ni2}, purple lines) coupling pathways. (c) Fragment of the structure highlighting the primary coordination sphere of the O_h Ni^{2+} centers with the two nearest-neighbor coupling pathways, J_{Ni1} and J_{Ni2}, denoted. (d) Ni^{2+}---X---Ni^{2+} fragments, highlighting the superexchange bridging angle. Brown, gray, green, yellow-tan, teal, blue, and red spheres are bromide, carbon, chloride, halide, nickel, nitrogen, and oxygen, respectively. Framework water molecules and hydrogens have been omitted for clarity.

studying this property in structurally disordered AFM/FM bilayer systems poses significant challenges.[35−37] Investigating such properties in well-defined spin-functional lattices is advantageous in furthering insights into the nature of the disorder in complex systems.

Spin frustration in antiferromagnetically coupled isotropic (Heisenberg) spin centers hosted on two-dimensional (2D) triangular and kagomé lattices composed of triangular plaquettes comprise the vast majority of studies in this space.[7,8,39−50] In these systems, frustration arises from the inability to satisfy all nearest-neighbor antiferromagnetic (AFM) interactions in the plaquettes as a consequence of the symmetry and geometry of the parent lattice. Creating a frustrated spin state on an AFM honeycomb lattice is challenging, as the geometry of the lattice enables the ordering of all isotropic spins, unlike that of a triangular or kagomé lattice.[51,52] Without additional interactions, antiferromagnetically coupled spins on a honeycomb lattice undergo long-range AFM order.[51,52]

We created spin frustration in a honeycomb lattice with nearest-neighbor interactions alternating between AFM and ferromagnetic (FM) (Figure 1a). Spins in this pattern on a honeycomb lattice generate frustration through competing interactions; nearest-neighbor AFM and FM interactions cannot be simultaneously satisfied, inducing frustration (Figure 1a). While most studies on frustrated spin physics have focused on materials with naturally occurring lattices, more recent advances have explored cold atoms or fabricated systems like magnetic nanostructures.[39−41,50,53−58] A chemical approach, such as metal−organic framework (MOF) based synthesis, allows for the designed construction of new materials.[59−62]

Many studies of magnetic MOFs feature a single linker to mediate magnetic exchange.[62,63] However, to achieve our desired frustrated lattice, we employed a mixed-linker approach, allowing for alternating interactions mediated by different linkers. In mixed-linker MOFs, alternating AFM and FM interactions have been realized by using bis(bidentate) organic ligands for AFM exchange and ambidentate azide-based linkers for FM exchange when coordinating end-on (EO).[64−67] The first example, reported by Cortés et al., involved an azidomanganges(II) honeycomb lattice where chains of O_h $S = 5/2$ Mn^{2+} ions connected by double EO azido bridges are linked by 2,2′-bipyrimidine ligands.[64] At high temperatures, dominant FM interactions facilitated by the azido bridges lead to pseudochain behavior, while at lower temperatures, the AFM interchain coupling via the bpym ligands results in long-range AFM order. While previous research on mixed-linker frameworks aimed to create molecular-based multifunctional materials,[64−67] our goal was to use this strategy to induce spin frustration in a honeycomb lattice.

As we build our systems from chemical components, we can tune the metal identity and, therefore, the spin state of our materials. Spin frustration is most commonly studied in systems with $S = 1/2$ centers,[39−41,50,53,54] in part because of the quantum nature of the spin system. Yet, the $S = 1$ case, which lies in an unusual quantum-classical middle ground, remains underexplored. Whether $S = 1$ systems can create materials with collective quantum properties remains an open question.[68−70] To investigate such systems, we selected O_h d^8 Ni^{2+} as a promising ion to host our $S = 1$ centers. To achieve an O_h coordination of our metal centers and the facilitation of a 2D honeycomb lattice, we selected the bidentate ligand pymca as our first ligand. Previously, pymca was used to mediate AFM coupling between O_h Ni^{2+} centers in a 2D honeycomb lattice,[71] making it a promising choice for mediating AFM interactions in our materials. To enforce FM coupling along our second coupling pathway, the linker must promote a 90° (or near 90°) alignment of our spin centers ($\angle Ni^{2+}$---L---Ni^{2+} ≈ 90°) for the spin-bearing 3d Ni^{2+}-based orbitals of the same symmetry (e_g) to interact.[72−74] To satisfy this requirement, we identified halides as an advantageous choice because there is literature precedent for FM coupling between O_h Ni^{2+} centers with $\angle Ni^{2+}$---X---Ni^{2+} ≈ 90°.[75,76] Furthermore, changing the identity of the halide influences the overlap between the spin-bearing 3d orbitals and the magnetic anisotropy of the system. This provides a chemical handle to tune the magnetism of our materials without compromising the overall structure.

Toward this end, we synthesized two novel metal−organic-based systems, $Ni_3(pymca)_3X_3{\cdot}nH_2O$ (NipymcaX; where X = Cl^- or Br^-). Two distinct nearest-neighbor coupling pathways mediate spin−spin interactions between the O_h $S = 1$ Ni^{2+} centers: J_{Ni1} via the organic pymca groups and J_{Ni2} via the inorganic halides. In both materials, the dominant interaction is J_{Ni1}, which is AFM in nature. Through chemical modification of the bridging halide group, we tune the magnitude of the FM interaction, J_{Ni2}, and the single-ion anisotropy of the Ni^{2+} spins. Although both materials are significantly frustrated, NipymcaCl is a topological (frustrated) spin glass, while NipymcaBr is

https://doi.org/10.1021/jacs.4c10113
J. Am. Chem. Soc. XXXX, XXX, XXX−XXX

a disordered spin system with a low-temperature exchange bias. As exchange bias is traditionally displayed by materials with a significant structural disorder, such as AFM/FM interfacial materials and nanostructured systems,[34−37] NipymcaBr is a rare example of a single-phase, well-ordered system exhibiting such a phenomenon.[22,23] Additionally, we use density functional theory (DFT) calculations and Monte Carlo (MC) simulations on the NipymcaX lattice to further interrogate the frustrated landscape of these materials, focusing on the ground-state spin configuration and finite-temperature spin−spin correlations. Since this NipymcaX system contains neutral layers, this class of materials is especially appropriate for future studies on the magnetic and electrical properties of physically exfoliated monolayers. In general, this introduction of the frustrated honeycomb lattice with alternating AFM and FM interactions using a metal−organic platform provides a highly modular route for the realization of exotic spin physics on traditionally challenging lattices.

■ RESULTS AND DISCUSSION

Synthesis, Structure, and Magnetostructural Correlations. To target the desired modified honeycomb phases, NipymcaX, we reacted Ni^{2+} hydrate salts with appropriate sources for our two linkers (2-cyanopyrimidine for pymca, $NiCl_2{\cdot}6H_2O$ for Cl^-, and $NiBr_2$ and KBr for Br^-) solvothermally at 130 °C (see the Experimental Section of Supporting Information for full details). After 21 h, we recovered green, plate-like crystals, which we identified to have the composition of $Ni_3(pymca)_3X_3{\cdot}nH_2O$ (see the Supporting Information for full characterization details). NipymcaCl and NipymcaBr both crystallize in the trigonal space group $P{-}3m1$ and are isostructural to each other (Tables S1 and S2). The layers (NipymcaX) are charge-balanced and consist of O_h Ni^{2+} sites that are bound in a *cis* configuration to two halides and two pymca groups (Figure 1b). We note these structures bear a similarity to the electronic Kekulé-O phase in graphene.[77−81] For a more detailed analysis of this comparison, we direct the reader to the discussion in Supporting Information.

There are two distinct coupling pathways between nearest-neighbor Ni^{2+} sites: J_{Ni1} via the pymca groups and J_{Ni2} via the halides (Figure 1c). Previously, coupling between $S = 1$ O_h Ni^{2+} centers mediated through pymca linkers was found to be AFM in nature.[71] In our systems, the nearest-neighbor Ni^{2+}---Ni^{2+} distances through the pymca ligands are 5.5161(7) Å in NipymcaCl and 5.4989(24) Å in NipymcaBr. As a result of these very similar distances, we expected the magnitude of the AFM coupling afforded by the pymca groups (J_{Ni1}) to be quite similar between the two materials.

The key difference between the materials lies in the halide bridge. Magnetic studies on O_h Ni^{2+}-based dimers with Cl and Br bridges mediating superexchange between the metal centers revealed an exchange that was FM in nature with bridging angles ($\angle Ni^{2+}$---X----Ni^{2+}) of 96.55° (Cl) and ca. 96° (Br).[75,82] In NipymcaCl and NipymcaBr, $\angle Ni^{2+}$---X----Ni^{2+} is 96.424(26)° (Cl) and 96.055(14)° (Br), respectively, within the range expected for FM exchange (Figure 1d). We anticipated that the FM coupling (J_{Ni2}) mediated by the Br atoms in NipymcaBr would be stronger than that through the Cl atoms in NipymcaCl. In NipymcaBr, the bridging angle of 96.055(14)° is closer to the ideal 90°, which maximizes FM coupling between spin-bearing orbitals of the same symmetry. Furthermore, the greater diffusivity of the 4p orbitals in Br compared to that of the 3p orbitals in Cl creates a more effective superexchange pathway, resulting in stronger coupling. This magnetostructural analysis suggests we designed honeycomb lattices with alternating AFM (J_{Ni1}) and FM coupling (J_{Ni2}) interactions (Figure 1b). We will thus interrogate the impact of the site-specific modulation of J_{Ni2} on the magnetism of NipymcaCl and NipymcaBr through experimental measurements and computational insight.

Bulk Magnetic Properties. To investigate the magnetic properties of our two materials, we started with dc susceptibility ($\chi_M T$) measurements on polycrystalline samples. (For a detailed discussion of all magnetic measurements, please refer to the "Full Experimental Details" section of the Supporting Information.) At room temperature, both $\chi_M T$ values agree with three unpaired $S = 1$ centers per formula unit ($\chi_M T \approx 3$ $cm^3K/mol{\cdot}Oe$, Figure 2). Fits in the high-temperature paramagnetic limit to the inverse susceptibility data (Tables S13 and S16 and Figures S22 and S38) reveal magnetic moments (μ_{eff}) characteristic of the O_h Ni^{2+} centers with moderate spin−orbit contributions (Cl: 3.23(1) and Br: 3.498(4) μ_B/Ni^{2+}). The spin centers in NipymcaBr are more anisotropic than those in NipymcaCl, which we attribute to the proximity of the heavier diamagnetic Br^- ion ($Z \approx 35$), relative to the Cl^- ion ($Z \approx 17$), to the spin moments. This phenomenon has been extensively studied in molecular complexes of first-row transition metal and is known as an effective strategy for enhancing the magnetic anisotropy of light metals.[83−86]

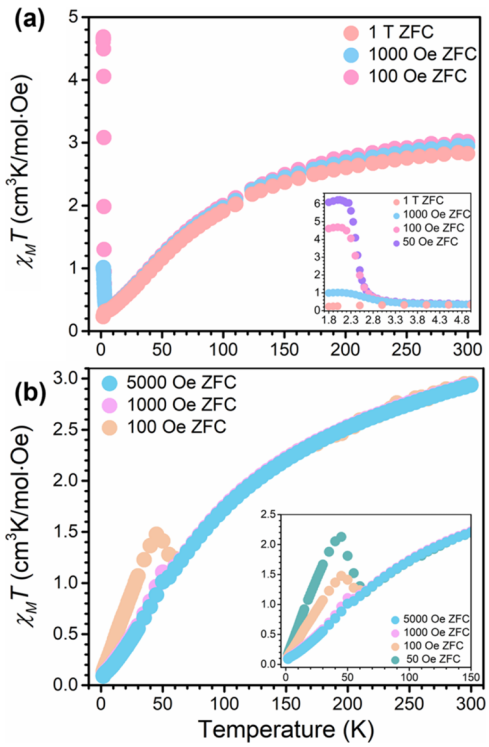

Figure 2. Bulk magnetic properties of NipymcaX. ZFC dc susceptibility data from 1.8 to 300 K, plotted as $\chi_M T$ vs T for (a) NipymcaCl. Inset: Data plotted from 1.8 to 5 K. (b) NipymcaBr. Inset: Data plotted from 1.8 to 150 K.

These fits also reveal dominant mean-field AFM interactions with Curie−Weiss temperatures (θ_{CW}) of −77 and −150 K for NipymcaCl and NipymcaBr, respectively. This AFM behavior persists as a downturn in the $\chi_M T$ susceptibility data as the

https://doi.org/10.1021/jacs.4c10113
J. Am. Chem. Soc. XXXX, XXX, XXX−XXX

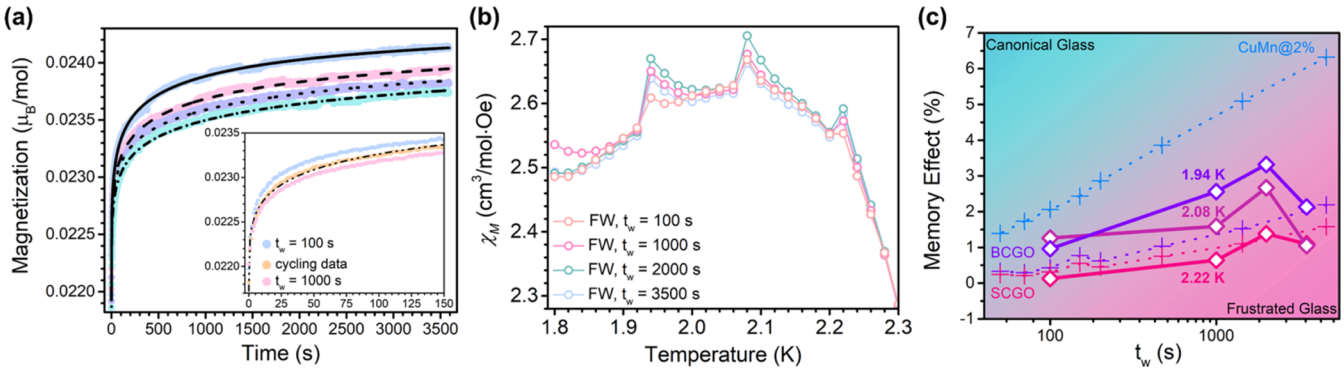

Figure 3. Bulk measurements of the spin glass behavior of NipymcaCl. (a) ZFC aging data with fits to the data (black lines). t_w = 100 s (pastel blue), 1000 s (pastel pink), 2000 s (pastel purple), and 3500 s (pastel green). **Inset:** ZFC cycling data with a fit (black line) to the data. Data were collected at 1.8 K with an applied field of 50 Oe. (b) FW susceptibility data of the memory effect were plotted from 1.8 to 2.3 K with an applied field of 50 Oe. (c) Plot comparing the quantified memory effect in NipymcaCl with simulations of the memory effect in literature materials. The data for the literature materials were taken from Samarakoon et al.[28] Colored lines are guides for the eye.

temperature is lowered from 300 K. Below 100 K, for NipymcaBr, $\chi_M T$ continues to generally trend toward zero, with the exception of a sharp, field strength-dependent feature around 50 K (Figure 2b inset). In contrast, NipymcaCl exhibits a gradual, field-dependent recovery of the $\chi_M T$ product below 3 K (Figure 2a inset). We attribute this behavior to spin canting of the predominantly AFM spins.

Spin canting occurs when spins deviate from perfect alignment along their axis, characterized by the spin-canting angle (α). This phenomenon arises due to antisymmetric interactions, such as Dzyaloshinskii-Moriya (DM), and single-ion anisotropy.[87−90] The presence of antisymmetric interactions necessitates a breaking of inversion symmetry in the material's crystal structure.[88,89] In NipymcaCl and NipymcaBr, which crystallize in the centrosymmetric space group P-3m1 and where the Ni-based magnetic moments exhibit inversion symmetry, DM interactions are negligible. Therefore, the primary cause of spin canting in NipymcaCl and NipymcaBr is single-ion anisotropy. This anisotropy results from both the influence of the heavy Cl^- and Br^- ions and the distorted O_h environments around the Ni^{2+} ions, parametrized by the theta parameter (θ).[91] In NipymcaCl and NipymcaBr, θ is 205 and 210°, respectively (Table S4), indicating a departure from ideal O_h symmetry (θ = 0°) and consequent recovery of second-order orbital angular momentum. The resulting spin-canting angles are small, parametrized as 2.4 and 1.2° in NipymcaCl and NipymcaBr, respectively, based on fits to the linear region of the low-temperature magnetization data (Figures S23 and S42). These values of α are comparable to those observed in other Ni^{2+} metal−organic-based spin-canted magnets.[92−94]

Around 2.4 K, below the temperature at which the spin-canted AFM phase of NipymcaCl exists, we observe bifurcation between the field-cooled (FC) and zero-field-cooled (ZFC) susceptibility traces at low field, which we attribute to a magnetic transition (Figure S26). To further probe this transition, we performed ac susceptibility measurements and note a frequency dependence in the data with pronounced asymmetry characteristic of spin glasses. As such, we calculated the Mydosh parameter (X = 0.0015)[95,96] (Figure S27) for these data and found this parameter fits within the characterization parameter for spin glasses (X = 0.002−0.1).[95−97] We therefore assign the transition at 2.36 K to a freezing transition (T_f), below which NipymcaCl exists as a spin glass.

Spin Glass Behavior of NipymcaCl. Spin glasses are an older class of materials that have undergone a recent renaissance. These materials provide a playground for studying spin dynamics; they exhibit frozen spin arrangements as a consequence of strong short-range interactions and are out-of-equilibrium, disordered systems.[95,96,98−100] The interplay of forces and the potential for dynamic spin configurations have reinvigorated interest in spin glasses, with particular emphasis on a class of spin glasses known as topological spin glasses.[22−28] To understand the nature of the glassy dynamics in NipymcaCl, we executed a standard set of experiments.

The first, which probes the complex dynamics of spin glasses, is an aging experiment. Aging is a fundamental process in out-of-equilibrium relaxation dynamics. It refers to the observation that relaxation − in this case, magnetic relaxation, τ − grows without a bound in time ("stiffens"), so the system under study looks slower as more time elapses (longer waiting time, t_w).[95,96,99,101] For our aging experiments on NipymcaCl, we followed a ZFC procedure (Figure S28a) and measured the magnetization of NipymcaCl as a function of time with different waiting times, t_w. The results of these experiments are shown in Figure 3a. Notably, the time-dependent behavior of the magnetization of NipymcaCl is modeled with a stretched exponential equation indicative of spin glass behavior to parametrize the glassy dynamics (see "Discussion of magnetic measurements" in the Supporting Information).[102] As NipymcaCl is aged, we observe a stiffening of τ on an experimental time scale, consistent with spin glass behavior (Table 1). Additionally, the aging of NipymcaCl corresponds to a decrease in the stretched exponential parameter, β. This β parameter represents the distribution of all possible relaxation pathways for a spin or a collection of spins in a material. For a slowly relaxing, well-defined system with discrete energy levels,

Table 1. Spin Glass Parameters Derived from Fitting the Aging and Cycling Curves of NipymcaCl Are Shown in Figure 3

t_w (s)	M_{SG} (μ_B/mol)	τ (s)	β
100	0.00245	200	0.273
1000	0.00246	433	0.247
2000	0.00247	646	0.228
3500	0.00278	1011	0.203
1000, 100	0.00246	256	0.286

https://doi.org/10.1021/jacs.4c10113
J. Am. Chem. Soc. XXXX, XXX, XXX−XXX

β is equal to 1, and for a system with no time dependence in the relaxation, β is 0. In spin glasses, β is an intermediate value between 0 and 1 because the energetic landscape is not well-defined and consists of many local minima potential energy wells.[100,101,103,104] As a spin glass aged, more of the spins traverse this rugged landscape and fall into metastable states, which shut down a portion of all of the possible relaxation pathways in the material. We observe this phenomenon in NipymcaCl; as it is aged, β decreases (Table 1).

Generally, glassy magnetic materials fall into one of two categories: canonical spin glasses or topological (frustrated) spin glasses. Canonical spin glasses are aptly named, as these were the initial magnetic materials for spin glass studies.[95,96,98] These materials are dilute magnetic alloys (i.e., CuMn) where a paramagnetic spin "impurity" is embedded in a nonmagnetic host, causing random magnetic interactions as a result of structural disorder. The glassiness in canonical spin glasses thus originates from this structural randomness. Contrastingly, the glassiness in topological spin glasses is the consequence of significant spin frustration in well-ordered, crystalline materials.[101,105,106] As a result, canonical and topological (frustrated) spin glasses have dissimilar energetic landscapes. While their landscapes are both rugged, the landscape in a canonical spin glass is a hierarchical one (funnel-shaped).[101] In this landscape, moving between different local minima incurs a rather large energy cost and requires a fair amount of external energy. When the amount of external energy given to a canonical glass is too low, the spins become trapped in a particular metastable state. The rugged landscape of a topological glass, however, is composed of nearly degenerate states and is nonhierarchical.[101] As there is a much lower energy penalty to move between states, accessing different states of a frustrated glass requires less energy, and spins are less likely to get trapped in a particular state.

An initial experiment to assess whether the energetic landscape of a spin glass is hierarchical or nonhierarchical is the cycling experiment. This experiment is similar to an aging experiment, except a small thermal cycle is added below T_f to assess how the system adapts to that perturbation. For specific details of the exact procedure that we performed, see Figure S28b. The resulting data from our cycling experiment on NipymcaCl are shown in the inset of Figure 3a (golden-rod dots) and are plotted against the noncycled (aging) data, which correspond to the two waiting times (100 and 1000 s) used in the cycling experiment. Conspicuously, the cycling data do not overlap with the noncycled data for either of the waiting times. Additionally, the magnetic parameters extracted from fitting the data are different from those for the initial aged experiments (Table 1). Cycling the spins of NipymcaCl enabled the acquisition of a state different from the original states expressed in the aging experiments. This suggests that the spins are more easily able to traverse the energetic landscape, indicative of a nonhierarchical landscape. Additionally, there are no inflection points in the first derivative of the aging data (Figure S29 inset), which further supports topological glass behavior.

The most infamous and mysterious phenomenon in spin glass behavior is memory.[101,107−109] To probe the memory effect in NipymcaCl, we performed a memory protocol (see Figure S31 for the full details). First, we cooled NipymcaCl from 10 K (above T_f) to below T_f. While cooling below T_f, we aged NipymcaCl at three equally spaced temperature points (2.22, 2.08, and 1.94 K). Upon reaching the base temperature of the instrument (1.8 K), we applied a small perturbative field of 50 Oe and collected a field-warmed (FW) susceptibility curve with continuous warming. While warming through the three temperatures at which the material was aged, NipymcaCl recovers the previous waiting time effect (Figure 3b). This is memory − NipymcaCl remembers that it was aged. On the other hand, when a temperature at which NipymcaCl was not aged is reached, it behaves as if there was no aging (the resulting FW susceptibility curve overlaps with the initial ZFC curve) during the cooling period (Figure S32). This phenomenon is referred to as "rejuvenation" or "temperature chaos." At these temperatures, NipymcaCl forgets that it was aged and appears "younger." We observe a series of rejuvenations and memories in the data, resulting in a sawtooth-like pattern, as shown in Figure 3b. The origin and nature of memory and rejuvenation in spin glasses have been the subject of intense investigation and controversy for decades.[101,109−112] Since this memory effect can be exploited to create switchable magnetic memory devices,[113,114] it is clear that a better understanding of the phenomenological process of such an effect is key to advancing such magnetic technologies.

We quantified the memory effect in NipymcaCl as a percentage (Figure S33) to compare to literature values. Figure 3c shows the effect at the three temperatures of aging as a function of waiting time (in log-scale) alongside computational data for three literature glasses: a canonical spin glass (CuMn@2%) and two topological spin glasses ($ACr_{9p}Ga_{12-9p}O_{19}$ where A = Sr^{2+}, Ba^{2+}).[101] In general, the memory effect in canonical spin glasses (1−10%) is about 1 order of magnitude larger than that (0.1 to 2−3%) in topological spin glasses.[101] Additionally, it is relatively linear with respect to waiting time, which is attributed to the hierarchical energetic landscape. Meanwhile, the memory effect of topological glasses does not have as linear of a trend. This is attributed to the nearly degenerate energetic landscape, which provides a nontrivial response to waiting time.[101,104]

In the context of these simulated data, the glassy behavior of NipymcaCl is more akin to that of topological spin glasses with a nonlinear trend in its memory effect and with a maximum effect of 3.4% (Figure 3c). Interestingly, the memory effect of NipymcaCl has a temperature dependence as well. The temperature at which the data for the literature materials were simulated is $T = 0.7T_f$, which is posited to be the temperature of maximum memory effect.[101,104] In NipymcaCl, this temperature is 1.7 K, below the base temperature of our PPMS, so we were unable to get memory data this cold. However, at the lowest temperature interrogated here (1.94 K), the magnitude of the memory effect trends toward a few percentages while remaining nonlinear with respect to waiting time. This suggests that the energetic landscape of NipymcaCl becomes more susceptible to environmental perturbations with decreasing temperature but retains nonhierarchical character. Understanding the complexity of the relaxation dynamics in spin glasses like NipymcaCl is a key challenge not only for understanding phenomenological physical processes but also for optimizing applications where the minimization of a complicated cost function is required, such as training artificial neural networks.[29−32]

Exchange Bias in NipymcaBr. Now, we turn toward a more thorough investigation of the magnetic properties of NipymcaBr. The sharpness of the previously described spin-canting transition at 50 K and the subsequent decrease in the $\chi_M T$ product are indicative of short-range order between the

https://doi.org/10.1021/jacs.4c10113
J. Am. Chem. Soc. XXXX, XXX, XXX−XXX

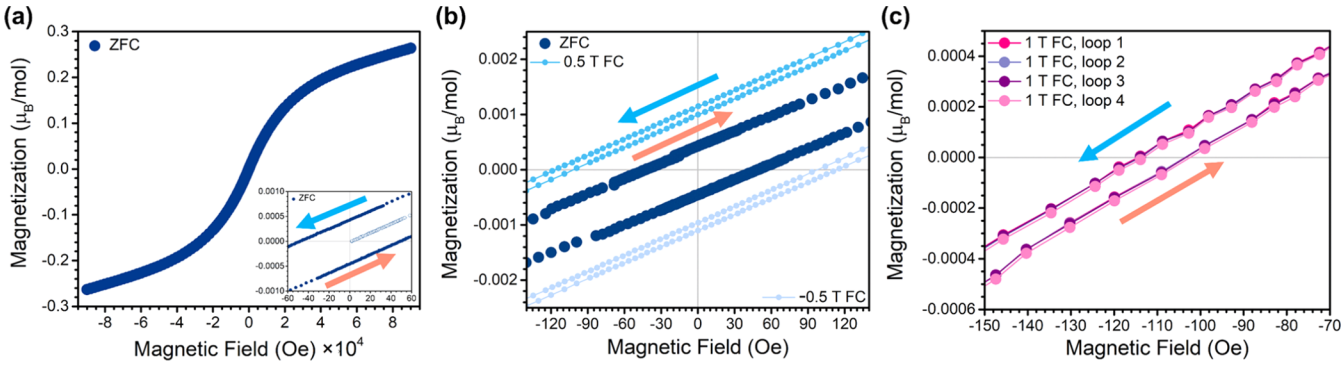

Figure 4. Characterizing the ground-state behavior of bulk NipymcaBr. (a) ZFC magnetization curve. Inset: Same data from −50 to 50 Oe to show hysteretic behavior. (b) Exchange bias behavior under FC conditions (0.5 T). (c) FC magnetization curves after cycling four times. All data were collected at 1.8 K. The arrows designate the field ramping (peach red) and deramping (sky blue) directions.

predominantly AFM spins. Additionally, the susceptibility data plotted as χ_M exhibits an upturn as the temperature is lowered (Figure S36), resembling a system with uncompensated magnetization. Despite the dominant AFM interactions promoting short-range order between the spin centers, the competing FM interactions mediated by the bromide linkers destabilize the formation of long-range AFM order. We observe no magnetic transitions in frequency-dependent ac susceptibility experiments at around 50 K (Figure S40). Furthermore, field-dependent heat capacity measurements (Figures S50 and S51) show no magnetic transitions down to 1.8 K, suggesting that NipymcaBr does not undergo long-range magnetic order and is a canted disordered magnet. The frustration parameter (f) for NipymcaBr, which is the ratio of the magnetic correlations approximated by θ_{CW} to an ordering (or magnetic) transition temperature (in this case, 1.8 K), is 81.8.[7] This is within the range of that reported for previously characterized spin frustrated materials[7,40,115] and is more than twice that of f in NipymcaCl (32.7), which we earlier identified to be a topological (frustrated) spin glass.

To better understand the ground-state properties of NipymcaBr, we performed low-temperature magnetization measurements. Magnetization experiments at 1.8 K reveal hysteretic behavior resulting from the uncompensated magnetization of the canted spins (Figure 4a). NipymcaBr is a soft magnetic material with an H_c of 27 Oe and a M_r of 0.00026 μ_B/mol. As the maximum value of magnetization (0.278 μ_B/fu) is 4.63% of the saturation magnetization (M_S) for a ferromagnet with three S = 1 centers, this substantiates the contribution of AFM correlations to the ground-state spin structure. The interplay between AFM and FM spin textures in materials has been extensively studied in materials with interfaces (i.e., AFM/FM interfacial or bilayer materials).[34,36,37] The exchange anisotropy created at the interfaces of the AFM/FM spin textures in these materials results in a phenomenon known as exchange bias.

In a normal ferromagnet, there are two equivalent collinear magnetization directions (+M and −M) along the easy axis of magnetization. Since the same external field strength is required to flip the magnetization from + M to − M and vice versa, the resulting magnetization loop is symmetric about zero field. When there is an AFM/FM interface, the magnetization loop after annealing in a magnetic field becomes asymmetric and shifts away from zero field.[40,42,43] There is now a new biased easy axis of magnetization for the ferromagnet created by the antiferromagnet pinning the magnetization of the ferromagnet in that direction. This pinning of the magnetization is achieved by the antiferromagnet exerting an exchange energy on the ferromagnet that is read-out as the exchange bias field, H_E.[34,36,37]

To test for the possibility of exchange bias in NipymcaBr, we cooled a sample under a variety of field strengths and recorded the subsequent magnetization curves (Figure 4b and Table S17). We see a marked shift in the magnetization loops of NipymcaBr relative to the initial ZFC curve (Figure 4b). Notably, there is exchange bias in NipymcaBr with an average H_E of −110 and H_c of 7.0 Oe (Table S17). Within error, the magnitude of H_E is independent of the applied field strength upon cooling. Additionally, the opposite exchange bias effect is measured (H_E = +106 Oe) when a negative cooling field is used, which is a hallmark effect in systems with exchange bias. Here, the H_c is smaller than that in the ZFC magnetization loop, which contrasts with the increase in coercivity commonly exhibited in AFM/FM interfacial materials with exchange bias.[34,36,37] In these systems, an increase in H_c is attributed to the antiferromagnet being weakly magnetically anisotropic.[34] When this is the case, during the flipping of the ferromagnet's magnetization, the ferromagnet's spins exert a force on the spins of the antiferromagnet and drag the spins to be in alignment. This results in more ferromagnetically aligned spins, which lead to a more coercive (harder) material. The decrease in H_c of NipymcaBr is reflective of the AFM component becoming more magnetically anisotropic when cooled under a field and resisting FM alignment. As a result, the coercivity of NipymcaBr decreases, and the material's magnetization softens.

Next, we performed isothermal induction experiments on NipymcaBr to ensure that the observed exchange bias is not a result of the minor loop phenomenon. Minor loops are closed hysteresis loops that occur when the applied magnetic field strength is not strong enough to effectively saturate the material and reverse the magnetization.[116] As a result, minor loops can exhibit asymmetry about zero field that is erroneously labeled as an exchange bias effect.[34] For our isothermal induction experiments, we cooled NipymcaBr under zero field to base temperature and then applied a field strength of 1 T for 1 h before recording the subsequent magnetization curves. This procedure resulted in magnetization loops with the same exchange bias effect previously observed with field cooling (Figure S44 and Table S17). As asymmetry in the minor magnetization loop of a material cannot be isothermally induced, this supports the exchange

https://doi.org/10.1021/jacs.4c10113
J. Am. Chem. Soc. XXXX, XXX, XXX−XXX

bias in NipymcaBr originating from the interaction of AFM and FM spin textures. Additionally, we selected cooling field strengths above the field necessary to effectively saturate the magnetization of NipymcaBr (overlapping of our field ramping and deramping curves, Figure 4a). This ensured that the resulting magnetization loops that we collected were major loops.

Systems with exchange bias can be magnetically trained to measure the evolution of the domain walls.[34] When a material exhibiting exchange bias is cycled (trained) under an applied field, H_E and H_c generally trend toward a constant value. This is the result of the domain walls in the material evolving from an initially perturbed FC state to an equilibrium state on the experimental time scale.[34] Magnetic training of NipymcaBr reveals that there is no change in the exchange bias effect as a function of cycle number (Figure 4c). This implies that by the time NipymcaBr is field-cooled to a base temperature, its domain walls have reached their steady-state energy configuration, suggesting that the external energy required for the movement of the domain walls is minimal. Furthermore, this equilibrium state is nonvolatile for a period of 1 h (Figure S46), which is promising for magnetoresistive random access memory applications that require a stable magnetic field readout.[117]

As exchange bias has been most commonly observed in materials with disordered AFM/FM interfaces,[34,36,37] the observed exchange bias in NipymcaBr is a rare example of this effect within a single-phase, crystalline material. The few known examples are kagomé-based materials[22,23] and a recently reported spin glass antiferromagnet.[118] In the kagomé materials, exchange bias arises from frustrated glassy dynamics driven by geometric frustration. Although the exact mechanism remains unknown, Murphy et al. suggest that exchange bias in such systems is an emergent phenomenon stemming from the interplay between magnetic field-induced chiral ordering and antisymmetric exchange.[23] This field-dependent chiral magnetic order has garnered both theoretical and experimental attention in kagomé antiferromagnets[119−121] and offers an intriguing parallel to the local ordering observed in topological spin glasses.[122−124] Within this framework, magnetic anisotropy and short-range spin ordering facilitate the development of locally correlated magnetically anisotropic spin textures. Upon application of a magnetic field, the anisotropic exchange interaction between the field and these textures polarizes the system and selects the chirality of these textures. The strength of the applied field dictates the proportion of spins within each texture, and because only a fraction of the spins reorient during a reverse field sweep, the hysteresis loop is shifted. We propose a similar origin for exchange bias in NipymcaBr, where the interaction of the magnetically anisotropic Ni^{2+} moments and short-range order in the system leads to the formation of locally correlated, magnetically anisotropic states. These states are thus susceptible to polarization and chiral selection under an applied field.

Exchange bias can be harnessed for future magnetic technologies, such as spintronics and information storage.[34,36,37] However, fabrication of quality AFM/FM interfacial thin films or nanostructures for such technologies is a pressing challenge in the field.[36,37] The advantage of NipymcaBr is that because it is single-phase, it exhibits exchange bias in the bulk. The neutrality of its layers suggests that it can be easily physically exfoliated for future device fabrication and integration studies. Additionally, the tunable MOF platform with which we designed NipymcaBr is tenable for the creation of materials with exchange bias at technologically relevant temperatures.

DFT Calculations and MC Simulations on NipymcaX. We supported the experimental observation of spin frustration in NipymcaX with DFT calculations and MC simulations (refer to Supporting Information). The DFT calculations were performed using the PBE functional, which does not account for relativistic effects such as spin−orbit coupling. Consequently, the calculated J values do not capture the differing single-ion anisotropies of the Ni^{2+} moments between NipymcaCl and NipymcaBr, which influences the materials' distinct magnetic properties. Despite this limitation, the DFT calculations validate alternating AFM (J_{Ni1}) and FM (J_{Ni2}) interactions in NipymcaX, with the magnitude of J_{Ni1} on the order of 100 K and that of J_{Ni2} on the order of 10 K, substantiating the dominant AFM interactions measured in the bulk susceptibility measurements, previously parametrized by a negative θ_{CW} (see the U_{eff} = 3 eV results in Table S18). Additionally, these calculations report moderately stronger FM interactions in NipymcaBr (J_{Ni2} = 19.14 K) compared to those in NipymcaCl (J_{Ni2} = 17.36 K), which supports our previous hypothesis that J_{Ni2} in NipymcaBr would be stronger than that in NipymcaCl.

MC simulations on the NipymcaX lattice support that alternating signs of J_{Ni1} and J_{Ni2} lead to spin frustration; same-sign coupling in either an AFM or an FM case leads to long-range magnetic order. Energy minimization of a supercell of 3D spin configurations with alternating AFM and FM correlations reveals that the maximum spin frustration is achieved when the ratio of J_{Ni2}/J_{Ni1} is −2, parametrized as x = 2/3 on the x-axis of Figure 5a (dotted line). This is noteworthy, as J_{Ni1} is twice as common in the lattice, so J_{Ni2} needs to be twice as strong for the system to be maximally frustrated. From the DFT calculations, J_{Ni1}/J_{Ni2} was determined to be −6.131 (x = 0.1402) in NipymcaCl and −5.689 (x = 0.1495) in NipymcaBr (Figure 5a). Both materials fall within the AFM-dominated regime, but NipymcaBr is more frustrated than NipymcaCl, aligning with the higher frustration parameter that we calculated from our magnetometry data. Additionally, NipymcaBr exhibited an exchange bias, which we posit is due to its spins being more magnetically anisotropic. This hypothesis aligns with previous reports suggesting that single-ion anisotropy can stabilize exchange bias in magnetic nanoparticles.[125−127]

Determining the ordered spin configuration of magnetic materials traditionally requires experimentally challenging neutron and X-ray scattering experiments.[90] Here, we leveraged MC simulations to derive the ordering pattern on the NipymcaX lattice, with the spin ground state of NipymcaBr illustrated as an example (Figure 5b). The likely ordering pattern consists of 30 and 150° separated spin moments lying along a plane over a $\sqrt{3} \times \sqrt{3}$ supercell, regardless of the parameter x. This means that the area (and volume) of this spin supercell is 3 times that of the crystallographic unit cell. Interestingly, MC simulations at various unit cell sizes supported the uniqueness of this classical ground state up to a global rotational state in all spins. This lack of ground-state degeneracy suggests that the T = 0 behavior of this system more closely resembles that of an antiferromagnet on a triangular lattice, relative to that on a kagomé lattice.[128−130] This is despite the fact that the lattice would be kagomé-like if the spins paired with the inorganic halides acted as one spin

https://doi.org/10.1021/jacs.4c10113
J. Am. Chem. Soc. XXXX, XXX, XXX−XXX

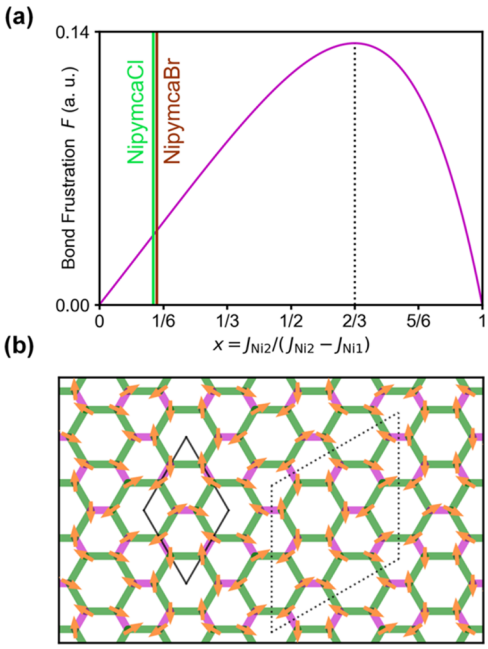

Figure 5. DFT and MC estimated energy frustration from Heisenberg-only interactions for NipymcaX and the ordering of NipymcaBr. (a) Bond frustration parameter (a) as defined in the Supporting Information − shown as a function of the ratio of Heisenberg couplings. Vertical bars indicate the positions of NipymcaBr and NipymcaCl in this plot based on DFT estimates of x as parametrized on the x-axis. (b) Likely 3D $\sqrt{3} \times \sqrt{3}$ ordering pattern of NipymcaBr given DFT estimated coupling parameters and MC-derived spin structure. Green bonds correspond to J_{Ni1} couplings and purple bonds to J_{Ni2} couplings. The solid boundary shows the crystal unit cell, while a dotted boundary indicates the unit cell of the spin ordering.

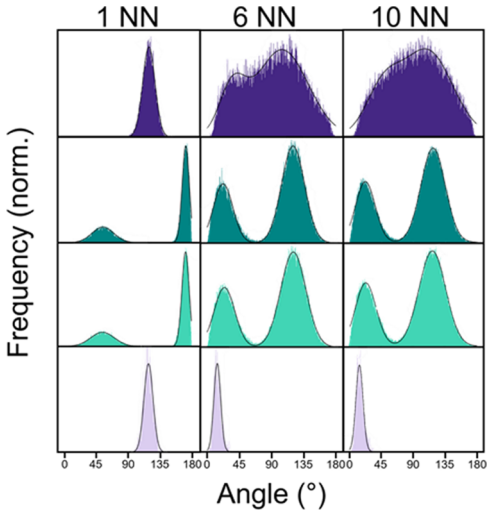

Figure 6. Results of the finite-temperature spin distributions for spins on the kagomé (dark purple simulations), NipymcaBr (dark green simulations), NipymcaCl (coral green simulations), and the triangular (pale lavender simulations) lattices, assuming nth nearest-neighbor (NN) interactions, parametrized as the full-width-max-height of the angular distributions from fitting the peaks to Gaussians. The NipymcaX lattice has 2 peaks since there are two symmetrically inequivalent interactions; we fit each individually.

center. Though one could expect a possible q = 0 ordering in the case of $J_{Ni2} \gg J_{Ni1}$, this turns out to be less energetically favorable over hexagonal plaquettes formed by J_{Ni1}-coupled bonds. In this limit, a quantum ($S = 1/2$) version of the system may exhibit more kagomé-like behavior.

Although the NipymcaX spin system supports only a single ground state, the existence of the two symmetrically distinct spin sites on this lattice, along with the competing J_{Ni1} and J_{Ni2} interactions, suggests that this system has the potential to host a more diverse distribution of spin configurations at finite temperatures when compared to a triangular lattice antiferromagnet. Semiclassical Markov chain Monte Carlo (MCMC) methods can simulate the finite-temperature properties by sampling from the Boltzmann distribution associated with the rugged landscape.[131,132] We implemented the Metropolis-Hastings algorithm on a network of $S = 1$ sites to model the distribution of spin configurations within our NipymcaX interface to compare to those within the AFM triangular and kagomé limit (Figure S53).[133] While holding the temperature constant at 1.8 K, we simulated the nth nearest-neighbor (NN) angle distribution on the NipymcaX lattice as well as on the AFM triangular and kagomé lattices for n = 1, 2, ... (where 11 is the limit of our simulations) and reported the results in Figures 6 and S53. For nth NN with spin moments ($\mathbf{S}_i$, $\mathbf{S}_j$) in a perfectly ordered system, we expect a sharply peaked distribution at the energy-minimizing angle between $\mathbf{S}_i$ and $\mathbf{S}_j$ of each symmetrically inequivalent interaction (i.e., 0 uncertainty), while for a disordered system, we expect a very broad distribution of the relative angle between two $S = 1$ moments selected uniformly at random (i.e., maximal uncertainty).

At low n (i.e., 1 NN), all three of the lattice types have low uncertainties about the energy-minimizing angle, reflective of short-range order in this low-temperature state (Figure 6). As n increases, the spin distribution within the kagomé lattice begins to approach an overall near-uniform distribution. In contrast, the spin distribution within the triangular lattice continues to be localized around a single angle difference at all simulated n, indicative of a longer-range order. The spin distribution in the NipymcaX lattice lies in an intermediate region between these two limits, with a broadening of the relative angle distribution in both competing interactions but converging to an angle peak uncertainty significantly below the uniform threshold (Figure S53). This suggests that the spins in NipymcaX are more ordered than those in an AFM kagomé lattice but have a much shorter-range ordering than that in an AFM triangular lattice despite having a unique thermodynamic ground state.

While undistorted AFM triangular and kagomé lattices are well-established and extensively studied,[7,8,39−50] our engineered system occupies an exciting intermediate region of glassiness. Such intermediate lattices have been theoretically explored in mixed-valent 2D organic polymers, which are emerging as promising platforms for quantum materials.[134] Lattices like NipymcaX not only represent a novel instance of frustrated magnetism but also mark an early step toward the discovery of more complex frustrated lattices with emergent properties beyond traditional paradigms. Additionally, the influence of single-ion anisotropy in NipymcaX underscores its potential to host a diverse range of physical phenomena arising from subtle variations in material properties.

As the experimentally determined heat capacities of NipymcaCl and NipymcaBr are convolutions of the magnetic, lattice, and phonon contributions, we turned toward similar simulations to extract the magnetic contribution to the heat

https://doi.org/10.1021/jacs.4c10113
J. Am. Chem. Soc. XXXX, XXX, XXX−XXX

capacity of NipymcaCl and NipymcaBr (Figure S53). Excitingly, simulations of the magnetic heat capacity revealed a macroscopic contribution at finite temperature, indicative of the disordered thermal fluctuations in the spin frustrated states. We note that the simulated magnetic heat capacities, when converted to the experimental units, are on the order of 50 J/molK at low temperatures, which is about 100× more than the experimental heat capacities. We attribute this to the glassy nature of the NipymcaX lattice where, as a consequence of the freezing of the disordered system, only a fraction of the overall number of spins contributes to the heat capacity. This has been reported in another spin glass material, where researchers discovered that the experimental contribution to the magnetic heat capacity in $LiZn_2V_3O_8$ is around 2−5% of the fully modeled value.[135] Regardless, the prospect of being able to simulate the magnetic contributions of the heat capacity of exotic spin systems, bypassing the experimental limitation of requiring a structurally analogous diamagnetic analogue, is crucial toward understanding the thermodynamic behavior of these systems.

■ CONCLUSIONS

We present a novel route to induce spin frustration on a modified honeycomb lattice with alternating nearest-neighbor AFM and FM interactions. Utilizing a MOF platform, we design two new materials, NipymcaCl and NipymcaBr, that are successful realizations of this goal. Despite the selective chemical modification of the halide linkers that mediate the FM interactions, the magnetic coupling strengths of these materials are quite similar. The key difference in their magnetic properties arises from their distinct magnetic anisotropies. This anisotropy leads to spin canting in both materials, with NipymcaCl exhibiting topological spin glass behavior and NipymcaBr displaying a low-temperature exchange bias.

Despite not accounting for single-ion anisotropy in the materials, DFT and MC calculations support the experimentally observed frustrated physics. MC simulations also provide insights into the ground-state spin structure and finite-temperature spin distributions, highlighting the power of this computational tool to elucidate complex spin structures. To build on these findings, future experiments will include both half-polarized and nonpolarized neutron scattering measurements. Half-polarized neutron scattering measurements will enable extraction of the magnetic susceptibility tensor for the O_h Ni^{2+} sites, providing further insight into the alignment of the magnetic moments. Meanwhile, nonpolarized measurements will further explore the short-range order in NipymcaBr. Given the significant effect of magnetic anisotropy on the magnetism of NipymcaCl and NipymcaBr, further investigation into this effect through monolayer and single-crystal magnetic torque studies is of great interest. These studies will not only provide additional clarity on the observations reported here but also facilitate the exfoliation of NipymcaCl and NipymcaBr monolayers for material optimization and future device fabrication.

The MOF platform we present here is particularly exciting due to its potential to extend beyond the materials we have discussed, NipymcaCl and NipymcaBr. For example, a Cu^{2+}-based system (or a similar $S = 1/2$ configuration) could serve as a quantum analogue, with our MC simulations suggesting that it would exhibit more kagomé-like physics. Additionally, altering the identity of the linkers enables fine-tuning of the coupling strengths beyond what we have achieved here. By changing the ligands, one can modulate both J_1 and J_2 and explore the relationship between them. Various inorganic ligands, such as cyanide (CN^-), isocyanide ($R-CN^-$), hydroxide (OH^-), and iodide (I^-), can serve as potential linkers to mediate the ferromagnetic J_2 interaction. Moving toward radical-based linkers could not only strengthen the coupling interactions but also unveil new magnetic behaviors. This site-selective control provided by our engineered lattice paves the way for the creation of future designer magnets with exotic spin physics.

■ ASSOCIATED CONTENT

Supporting Information

The Supporting Information is available free of charge at https://pubs.acs.org/doi/10.1021/jacs.4c10113.

Full experimental details and data analysis, complete crystallographic data, additional figures of data, and details about DFT calculations and MC simulations. (PDF)

Further discussion of the MC simulations and results. (PDF)

Accession Codes

CCDC 2373021 and 2373022 contain the supplementary crystallographic data for this paper. These data can be obtained free of charge via www.ccdc.cam.ac.uk/data_request/cif, or by emailing data_request@ccdc.cam.ac.uk, or by contacting The Cambridge Crystallographic Data Center, 12 Union Road, Cambridge CB2 1EZ, UK; fax: +44 1223 336033.

■ AUTHOR INFORMATION

Corresponding Author

Danna E. Freedman − *Department of Chemistry, Massachusetts Institute of Technology, Cambridge, Massachusetts 02139, United States;* orcid.org/0000-0002-2579-8835; Email: danna@mit.edu

Authors

Stephanie M. Amtry − *Department of Chemistry, Massachusetts Institute of Technology, Cambridge, Massachusetts 02139, United States*

Arthur C. Campello − *Department of Applied Physics, Stanford University, Stanford, California 94305, United States; Stanford Institute for Materials and Energy Sciences, SLAC National Accelerator Laboratory, Menlo Park, California 94025, United States*

Christopher L. Tong − *Department of Chemistry, Massachusetts Institute of Technology, Cambridge, Massachusetts 02139, United States; Department of Physics, Massachusetts Institute of Technology, Cambridge, Massachusetts 02139, United States*

Danilo S. Puggioni − *Department of Materials Science and Engineering, Northwestern University, Evanston, Illinois 60208, United States*

James M. Rondinelli − *Department of Materials Science and Engineering, Northwestern University, Evanston, Illinois 60208, United States;* orcid.org/0000-0003-0508-2175

Young S. Lee − *Department of Applied Physics, Stanford University, Stanford, California 94305, United States; Stanford Institute for Materials and Energy Sciences, SLAC National Accelerator Laboratory, Menlo Park, California 94025, United States*

Complete contact information is available at:

https://pubs.acs.org/10.1021/jacs.4c10113

Funding

S.M.A. acknowledges funding from the Center for Molecular Quantum Transduction (CMQT) program supported by the Department of Energy Office of Science, Basic Energy Sciences (DE-SC0021314). D.S.P. and J.M.R. were supported by the National Science Foundation (NSF) through Award Number DMR-2413680. The work at Stanford and SLAC in the Stanford Institute for Materials and Energy Sciences (SIMES) was supported by the U.S. Department of Energy (DOE), Office of Science, Basic Energy Sciences (BES), Materials Sciences and Engineering Division, under Contract No. DE-AC02-76SF00515. This work made use of the IMSERC facility at Northwestern University, which has received support from Northwestern University, the State of Illinois, and the International Institute of Nanotechnology. This work was supported by the NSF through the MIT MRL at the MRSEC facility under Award Number DMR-1419807.

Notes

The authors declare no competing financial interest.

■ ACKNOWLEDGMENTS

The authors would like to thank Rianna B. Greer, Dr. Ryan A. Murphy, and Dr. Michael K. Wojnar for insightful discussions during the preparation of this manuscript.

■ ABBREVIATIONS

2D, two-dimensional; MOF, metal−organic framework; NipymcaX, pymca = pyrimidine-2-carboxylato and X = Cl^-, Br^-; *J*, magnetic coupling; AFM, antiferromagnetic; FiM, ferrimagnetic; FM, ferromagnetic; O_h, octahedral; χ_M, molar magnetic susceptibility; θ_{CW}, Curie−Weiss parameter; FC, field-cooled; ZFC, zero-field-cooled; T_f, freezing transition; t_w, waiting time; β, stretched exponential parameter; *f*, frustration parameter; *M*, molar magnetization; H_E, exchange bias field; H_C, critical field; DFT, density functional theory; MC, Monte Carlo; MCMC, Semiclassical Markov chain Monte Carlo; DM, Dzyaloshinskii-Moriya

■ REFERENCES

(1) Nielsen, A. E. B.; Sierra, G.; Cirac, J. I. Local Models of Fractional Quantum Hall States in Lattices and Physical Implementation. *Nat. Commun.* **2013**, *4* (1), No. 2864.

(2) Bauer, B.; Cincio, L.; Keller, B. P.; Dolfi, M.; Vidal, G.; Trebst, S.; Ludwig, A. W. W. Chiral Spin Liquid and Emergent Anyons in a Kagome Lattice Mott Insulator. *Nat. Commun.* **2014**, *5* (1), No. 5137.

(3) Wietek, A.; Läuchli, A. M. Chiral Spin Liquid and Quantum Criticality in Extended $S = 1/2$ Heisenberg Models on the Triangular Lattice. *Phys. Rev. B* **2017**, *95* (3), No. 035141.

(4) Huang, Y.; Zhu, W.; Gong, S.-S.; Jiang, H.-C.; Sheng, D. N. Coexistence of Non-Abelian Chiral Spin Liquid and Magnetic Order in a Spin-1 Antiferromagnet. *Phys. Rev. B* **2022**, *105* (15), No. 155104.

(5) Hu, W.-J.; Gong, S.-S.; Zhu, W.; Sheng, D. N. Competing Spin-Liquid States in the Spin-1/2 Heisenberg Model on the Triangular Lattice. *Phys. Rev. B* **2015**, *92* (14), No. 140403.

(6) Anderson, P. W. Resonating Valence Bonds: A New Kind of Insulator? *Mater. Res. Bull.* **1973**, *8* (2), 153−160.

(7) Ramirez, A. P. Strongly Geometrically Frustrated Magnets. *Annu. Rev. Mater. Sci.* **1994**, *24* (1), 453−480.

(8) Balents, L. Spin Liquids in Frustrated Magnets. *Nature* **2010**, *464* (7286), 199−208.

(9) Savary, L.; Balents, L. Quantum Spin Liquids: A Review. *Rep. Prog. Phys.* **2017**, *80* (1), No. 016502.

(10) Broholm, C.; Cava, R. J.; Kivelson, S. A.; Nocera, D. G.; Norman, M. R.; Senthil, T. Quantum Spin Liquids. *Science* **2020**, *367* (6475), No. eaay0668.

(11) Nemoto, R.; Arafune, R.; Nakano, S.; Tsuchiizu, M.; Takagi, N.; Suizu, R.; Uchihashi, T.; Awaga, K. Chiral Honeycomb Lattices of Nonplanar π-Conjugated Supramolecules with Protected Dirac and Flat Bands. *ACS Nano* **2024**, *18*, 19663−19671.

(12) Semeghini, G.; Levine, H.; Keesling, A.; Ebadi, S.; Wang, T. T.; Bluvstein, D.; Verresen, R.; Pichler, H.; Kalinowski, M.; Samajdar, R.; Omran, A.; Sachdev, S.; Vishwanath, A.; Greiner, M.; Vuletić, V.; Lukin, M. D. Probing Topological Spin Liquids on a Programmable Quantum Simulator. *Science* **2021**, *374* (6572), 1242−1247.

(13) Nayak, C.; Simon, S. H.; Stern, A.; Freedman, M.; Sarma, S. D. Non-Abelian Anyons and Topological Quantum Computation. *Rev. Mod. Phys.* **2008**, *80* (3), 1083−1159.

(14) Kitaev, A. Yu. Fault-Tolerant Quantum Computation by Anyons. *Ann. Phys.* **2003**, *303* (1), 2−30.

(15) Anderson, P. W. The Resonating Valence Bond State in La_2CuO_4 and Superconductivity. *Science* **1987**, *235* (4793), 1196−1198.

(16) Lee, P. A. From High Temperature Superconductivity to Quantum Spin Liquid: Progress in Strong Correlation Physics. *Rep. Prog. Phys.* **2008**, *71* (1), No. 012501.

(17) Imajo, S.; Sugiura, S.; Akutsu, H.; Kohama, Y.; Isono, T.; Terashima, T.; Kindo, K.; Uji, S.; Nakazawa, Y. Extraordinary π-Electron Superconductivity Emerging from a Quantum Spin Liquid. *Phys. Rev. Res.* **2021**, *3* (3), No. 033026.

(18) Kwon, H. Y.; Yoon, H. G.; Park, S. M.; Lee, D. B.; Shi, D.; Wu, Y. Z.; Choi, J. W.; Won, C. Searching for the Ground State of Complex Spin-Ice Systems Using Deep Learning Techniques. *Sci. Rep.* **2022**, *12* (1), No. 15026.

(19) Tellez-Mora, A.; He, X.; Bousquet, E.; Wirtz, L.; Romero, A. H. Systematic Determination of a Material's Magnetic Ground State from First Principles. *npj Comput. Mater.* **2024**, *10* (1), 20.

(20) Virtanen, P.; Gommers, R.; Oliphant, T. E.; Haberland, M.; Reddy, T.; Cournapeau, D.; Burovski, E.; Peterson, P.; Weckesser, W.; Bright, J.; Van Der Walt, S. J.; Brett, M.; Wilson, J.; Millman, K. J.; Mayorov, N.; Nelson, A. R. J.; Jones, E.; Kern, R.; Larson, E.; Carey, C. J.; Polat, İ.; Feng, Y.; Moore, E. W.; VanderPlas, J.; Laxalde, D.; Perktold, J.; Cimrman, R.; Henriksen, I.; Quintero, E. A.; Harris, C. R.; Archibald, A. M.; Ribeiro, A. H.; Pedregosa, F.; Van Mulbregt, P.; Vijaykumar, A.; Bardelli, A. P.; Rothberg, A.; Hilboll, A.; Kloeckner, A.; Scopatz, A.; Lee, A.; Rokem, A.; Woods, C. N.; Fulton, C.; Masson, C.; Häggström, C.; Fitzgerald, C.; Nicholson, D. A.; Hagen, D. R.; Pasechnik, D. V.; Olivetti, E.; Martin, E.; Wieser, E.; Silva, F.; Lenders, F.; Wilhelm, F.; Young, G.; Price, G. A.; Ingold, G.-L.; Allen, G. E.; Lee, G. R.; Audren, H.; Probst, I.; Dietrich, J. P.; Silterra, J.; Webber, J. T.; Slavič, J.; Nothman, J.; Buchner, J.; Kulick, J.; Schönberger, J. L.; De Miranda Cardoso, J. V.; Reimer, J.; Harrington, J.; Rodríguez, J. L. C.; Nunez-Iglesias, J.; Kuczynski, J.; Tritz, K.; Thoma, M.; Newville, M.; Kümmerer, M.; Bolingbroke, M.; Tartre, M.; Pak, M.; Smith, N. J.; Nowaczyk, N.; Shebanov, N.; Pavlyk, O.; Brodtkorb, P. A.; Lee, P.; McGibbon, R. T.; Feldbauer, R.; Lewis, S.; Tygier, S.; Sievert, S.; Vigna, S.; Peterson, S.; More, S.; Pudlik, T.; Oshima, T.; Pingel, T. J.; Robitaille, T. P.; Spura, T.; Jones, T. R.; Cera, T.; Leslie, T.; Zito, T.; Krauss, T.; Upadhyay, U.; Halchenko, Y. O.; Vázquez-Baeza, Y. SciPy 1.0: Fundamental Algorithms for Scientific Computing in Python. *Nat. Methods* **2020**, *17* (3), 261−272.

(21) Remund, K.; Pohle, R.; Akagi, Y.; Romhányi, J.; Shannon, N. Semi-Classical Simulation of Spin-1 Magnets. *Phys. Rev. Res.* **2022**, *4* (3), No. 033106.

(22) Lachman, E.; Murphy, R. A.; Maksimovic, N.; Kealhofer, R.; Haley, S.; McDonald, R. D.; Long, J. R.; Analytis, J. G. Exchange Biased Anomalous Hall Effect Driven by Frustration in a Magnetic Kagome Lattice. *Nat. Commun.* **2020**, *11* (1), No. 560.

(23) Murphy, R. A.; Darago, L. E.; Ziebel, M. E.; Peterson, E. A.; Zaia, E. W.; Mara, M. W.; Lussier, D.; Velasquez, E. O.; Shuh, D. K.; Urban, J. J.; Neaton, J. B.; Long, J. R. Exchange Bias in a Layered Metal−Organic Topological Spin Glass. *ACS Cent. Sci.* **2021**, *7* (8), 1317−1326.

(24) Shi, Y.; Nisoli, C.; Chern, G.-W. Ice, Glass, and Solid Phases in Artificial Spin Systems with Quenched Disorder. *Appl. Phys. Lett.* **2021**, *118* (12), No. 122407.

(25) Sen, A.; Moessner, R. Topological Spin Glass in Diluted Spin Ice. *Phys. Rev. Lett.* **2015**, *114* (24), No. 247207.

(26) Reissner, M. Mössbauer Spectroscopy in External Magnetic Fields. In *Modern Mössbauer Spectroscopy*; Yoshida, Y.; Langouche, G., Eds.; Springer Singapore: Singapore, 2021; Vol. *137*, pp 381−444.

(27) McCloy, J. S. Spin and Ferroic Glasses. In *Springer Handbook of Glass*; Musgraves, J. D.; Hu, J.; Calvez, L., Eds.; Springer International Publishing: Cham, 2019; pp 687−718.

(28) Bowman, D. F.; Cemal, E.; Lehner, T.; Wildes, A. R.; Mangin-Thro, L.; Nilsen, G. J.; Gutmann, M. J.; Voneshen, D. J.; Prabhakaran, D.; Boothroyd, A. T.; Porter, D. G.; Castelnovo, C.; Refson, K.; Goff, J. P. Role of Defects in Determining the Magnetic Ground State of Ytterbium Titanate. *Nat. Commun.* **2019**, *10* (1), No. 637.

(29) Anderson, P. W. Spin Glass IV: Glimmerings of Trouble. *Phys. Today* **1988**, *41* (9), 9−11.

(30) Albert, R.; Barabási, A.-L. Statistical Mechanics of Complex Networks. *Rev. Mod. Phys.* **2002**, *74* (1), 47−97.

(31) Mezard, M.; Parisi, G.; Virasoro, M. A. *Spin Glass Theory and Beyond*; World Scientific: Singapore, 2004.

(32) Introduction: Why Spin Glasses?. In *Spin Glasses and Complexity*; Princeton University Press, 2013; pp 1−14.

(33) Meiklejohn, W. H.; Bean, C. P. New Magnetic Anisotropy. *Phys. Rev.* **1956**, *102* (5), 1413−1414.

(34) Nogués, J.; Schuller, I. K. Exchange Bias. *J. Magn. Magn. Mater.* **1999**, *192* (2), 203−232.

(35) O'Grady, K.; Fernandez-Outon, L. E.; Vallejo-Fernandez, G. A New Paradigm for Exchange Bias in Polycrystalline Thin Films. *J. Magn. Magn. Mater.* **2010**, *322* (8), 883−899.

(36) Blachowicz, T.; Ehrmann, A. Exchange Bias in Thin Films—An Update. *Coatings* **2021**, *11* (2), 122.

(37) Blachowicz, T.; Ehrmann, A.; Wortmann, M. Exchange Bias in Nanostructures: An Update. *Nanomaterials* **2023**, *13* (17), 2418.

(38) Gider, S.; Runge, B.-U.; Marley, A. C.; Parkin, S. S. P. The Magnetic Stability of Spin-Dependent Tunneling Devices. *Science* **1998**, *281* (5378), 797−799.

(39) Nocera, D. G.; Bartlett, B. M.; Grohol, D.; Papoutsakis, D.; Shores, M. P. Spin Frustration in 2D Kagomé Lattices: A Problem for Inorganic Synthetic Chemistry. *Chem. − Eur. J.* **2004**, *10* (16), 3850−3859.

(40) Norman, M. R. *Colloquium*: Herbertsmithite and the Search for the Quantum Spin Liquid. *Rev. Mod. Phys.* **2016**, *88* (4), No. 041002.

(41) Chamorro, J. R.; McQueen, T. M.; Tran, T. T. Chemistry of Quantum Spin Liquids. *Chem. Rev.* **2021**, *121* (5), 2898−2934.

(42) Shores, M. P.; Nytko, E. A.; Bartlett, B. M.; Nocera, D. G. A Structurally Perfect $S = {}^1/_2$ Kagomé Antiferromagnet. *J. Am. Chem. Soc.* **2005**, *127* (39), 13462−13463.

(43) Helton, J. S.; Matan, K.; Shores, M. P.; Nytko, E. A.; Bartlett, B. M.; Yoshida, Y.; Takano, Y.; Suslov, A.; Qiu, Y.; Chung, J.-H.; Nocera, D. G.; Lee, Y. S. Spin Dynamics of the Spin-1/2 Kagome Lattice Antiferromagnet $ZnCu_3(OH)_6Cl_2$. *Phys. Rev. Lett.* **2007**, *98* (10), No. 107204.

(44) Matan, K.; Helton, J. S.; Grohol, D.; Nocera, D. G.; Wakimoto, S.; Kakurai, K.; Lee, Y. S. Polarized Neutron Scattering Studies of the Kagomé Lattice Antiferromagnet. *Physica B* **2009**, *404* (17), 2529−2531.

(45) Freedman, D. E.; Han, T. H.; Prodi, A.; Müller, P.; Huang, Q.-Z.; Chen, Y.-S.; Webb, S. M.; Lee, Y. S.; McQueen, T. M.; Nocera, D. G. Site Specific X-Ray Anomalous Dispersion of the Geometrically Frustrated Kagomé Magnet, Herbertsmithite, $ZnCu_3(OH)_6Cl_2$. *J. Am. Chem. Soc.* **2010**, *132* (45), 16185−16190.

(46) Smaha, R. W.; He, W.; Jiang, J. M.; Wen, J.; Jiang, Y.-F.; Sheckelton, J. P.; Titus, C. J.; Wang, S. G.; Chen, Y.-S.; Teat, S. J.; Aczel, A. A.; Zhao, Y.; Xu, G.; Lynn, J. W.; Jiang, H.-C.; Lee, Y. S. Materializing Rival Ground States in the Barlowite Family of Kagome Magnets: Quantum Spin Liquid, Spin Ordered, and Valence Bond Crystal States. *npj Quantum Mater.* **2020**, *5* (1), 23.

(47) Smaha, R. W.; Boukahil, I.; Titus, C. J.; Jiang, J. M.; Sheckelton, J. P.; He, W.; Wen, J.; Vinson, J.; Wang, S. G.; Chen, Y.-S.; Teat, S. J.; Devereaux, T. P.; Das Pemmaraju, C.; Lee, Y. S. Site-Specific Structure at Multiple Length Scales in Kagome Quantum Spin Liquid Candidates. *Phys. Rev. Mater.* **2020**, *4* (12), No. 124406.

(48) Wang, J.; Yuan, W.; Singer, P. M.; Smaha, R. W.; He, W.; Wen, J.; Lee, Y. S.; Imai, T. Emergence of Spin Singlets with Inhomogeneous Gaps in the Kagome Lattice Heisenberg Antiferromagnets Zn-Barlowite and Herbertsmithite. *Nat. Phys.* **2021**, *17* (10), 1109−1113.

(49) Wang, J.; Yuan, W.; Singer, P. M.; Smaha, R. W.; He, W.; Wen, J.; Lee, Y. S.; Imai, T. Freezing of the Lattice in the Kagome Lattice Heisenberg Antiferromagnet Zn-Barlowite $ZnCu_3(OD)_6FBr$. *Phys. Rev. Lett.* **2022**, *128* (15), No. 157202.

(50) Clark, L.; Abdeldaim, A. H. Quantum Spin Liquids from a Materials Perspective. *Annu. Rev. Mater. Res.* **2021**, *51* (1), 495−519.

(51) Auerbach, A. *Interacting Electrons and Quantum Magnetism*; Springer: New York, 1998.

(52) Xiao, R.-C.; Shao, D.-F.; Li, Y.-H.; Jiang, H. Spin Photogalvanic Effect in Two-Dimensional Collinear Antiferromagnets. *npj Quantum Mater.* **2021**, *6* (1), 35.

(53) Takagi, H.; Takayama, T.; Jackeli, G.; Khaliullin, G.; Nagler, S. E. Concept and Realization of Kitaev Quantum Spin Liquids. *Nat. Rev. Phys.* **2019**, *1* (4), 264−280.

(54) Trebst, S. Kitaev Materials 2017 http://arxiv.org/abs/1701.07056 (accessed May 07, 2022).

(55) Chern, G.-W. Artificial Spin Ice: Beyond Pyrochlores and Magnetism. In *Spin Ice*; Udagawa, M.; Jaubert, L., Eds.; Springer International Publishing: Cham, 2021; Vol. *197*, pp 419−453.

(56) Nisoli, C.; Moessner, R.; Schiffer, P. *Colloquium*: Artificial Spin Ice: Designing and Imaging Magnetic Frustration. *Rev. Mod. Phys.* **2013**, *85* (4), 1473−1490.

(57) Rougemaille, N.; Canals, B. Cooperative Magnetic Phenomena in Artificial Spin Systems: Spin Liquids, Coulomb Phase and Fragmentation of Magnetism − a Colloquium. *Eur. Phys. J. B* **2019**, *92* (3), 62.

(58) Barbiero, L.; Cabedo, J.; Lewenstein, M.; Tarruell, L.; Celi, A. Frustrated Magnets without Geometrical Frustration in Bosonic Flux Ladders. *Phys. Rev. Res.* **2023**, *5* (4), No. L042008.

(59) Rowsell, J. L. C.; Yaghi, O. M. Metal−Organic Frameworks: A New Class of Porous Materials. *Microporous Mesoporous Mater.* **2004**, *73* (1−2), 3−14.

(60) Yaghi, O. M.; O'Keeffe, M.; Ockwig, N. W.; Chae, H. K.; Eddaoudi, M.; Kim, J. Reticular Synthesis and the Design of New Materials. *Nature* **2003**, *423* (6941), 705−714.

(61) Butova, V. V.; Soldatov, M. A.; Guda, A. A.; Lomachenko, K. A.; Lamberti, C. Metal-Organic Frameworks: Structure, Properties, Methods of Synthesis and Characterization. *Russ. Chem. Rev.* **2016**, *85* (3), 280−307.

(62) Thorarinsdottir, A. E.; Harris, T. D. Metal−Organic Framework Magnets. *Chem. Rev.* **2020**, *120* (16), 8716−8789.

(63) Mínguez Espallargas, G.; Coronado, E. Magnetic Functionalities in MOFs: From the Framework to the Pore. *Chem. Soc. Rev.* **2018**, *47* (2), 533−557.

(64) Cortés, R.; Lezama, L.; Rojo, T.; Pizarro, J. L.; Arriortua, M. I. Alternating Ferro- and Antiferromagnetic Interactions in Honeycomb-Like Layers of an Azidomanganese(II) Compound. *Angew. Chem., Int. Ed.* **1996**, *35* (16), 1810−1812.

(65) Escuer, A.; Cano, J.; Goher, M. A. S.; Journaux, Y.; Lloret, F.; Mautner, F. A.; Vicente, R. Synthesis, Structural Characterization, and Monte Carlo Simulation of the Magnetic Properties of Two New Alternating Mn^{II} Azide 2-D Honeycombs. Study of the Ferromagnetic Ordered Phase below 20 K. *Inorg. Chem.* **2000**, *39* (21), 4688−4695.

https://doi.org/10.1021/jacs.4c10113
J. Am. Chem. Soc. XXXX, XXX, XXX−XXX

(66) Escuer, A.; Vicente, R.; Goher, M. A. S.; Mautner, F. A. A New Family of High-Dimensional Molecular Magnets Built from the Manganese−Azido System. Syntheses, Structures, and Magnetic Characterization of Two New Ferro−Antiferromagnetic Two-Dimensional Complexes. *Inorg. Chem.* **1997**, *36* (16), 3440−3446.

(67) Marino, N.; Armentano, D.; De Munno, G.; Lloret, F.; Cano, J.; Julve, M. Towards a Better Understanding of Honeycomb Alternating Magnetic Networks. *Dalton Trans.* **2015**, *44* (24), 11040−11051.

(68) Koga, A.; Kawakami, N. Frustrated Heisenberg Antiferromagnet on the Pyrochlore Lattice. *Phys. Rev. B* **2001**, *63* (14), No. 144432.

(69) Yamashita, Y.; Ueda, K.; Sigrist, M. Parity-Broken Ground State for the Spin-1 Pyrochlore Antiferromagnet. *J. Phys.: Condens. Matter* **2001**, *13* (50), L961−L967.

(70) Pati, S. K.; Rao, C. N. R. Role of the Spin Magnitude of the Magnetic Ion in Determining the Frustration and Low-Temperature Properties of Kagome Lattices. *J. Chem. Phys.* **2005**, *123* (23), No. 234703.

(71) Honda, Z.; Kodama, T.; Hagiwara, M.; Kida, T.; Okutani, A.; Sakai, M.; Fukuda, T.; Kamata, N. Crystal Structures and Magnetic Properties of the Honeycomb-Lattice Antiferromagnet M2(Pymca)-3(ClO4), (M = Fe, Co, Ni). *Solid State Sci.* **2016**, *59*, 15−18.

(72) Goodenough, J. B. Theory of the Role of Covalence in the Perovskite-Type Manganites [La,M(II)]MnO_3. *Phys. Rev.* **1955**, *100* (2), 564−573.

(73) Goodenough, J. B. An Interpretation of the Magnetic Properties of the Perovskite-Type Mixed Crystals $La_{1-x}Sr_xCoO_{3-\lambda}$. *J. Phys. Chem. Solids* **1958**, *6* (2−3), 287−297.

(74) Kanamori, J. Superexchange Interaction and Symmetry Properties of Electron Orbitals. *J. Phys. Chem. Solids* **1959**, *10* (2−3), 87−98.

(75) Joung, K. O.; O'Connor, C. J.; Sinn, E.; Carlin, R. L. Structural and Magnetic Properties of Dimeric Di-.Mu.-Chloro-Tetrakis-(Ethylenediamine)Dinickel(II) Chloride. *Inorg. Chem.* **1979**, *18* (3), 804−808.

(76) Ginsberg, A. P.; Martin, R. L.; Brookes, R. W.; Sherwood, R. C. Magnetic Exchange in Transition Metal Complexes. IX. Dimeric Nickel(II)-Ethylenediamine Complexes. *Inorg. Chem.* **1972**, *11* (12), 2884−2889.

(77) Qu, A. C.; Nigge, P.; Link, S.; Levy, G.; Michiardi, M.; Spandar, P. L.; Matthé, T.; Schneider, M.; Zhdanovich, S.; Starke, U.; Gutiérrez, C.; Damascelli, A. Ubiquitous Defect-Induced Density Wave Instability in Monolayer Graphene. *Sci. Adv.* **2022**, *8* (23), No. eabm5180.

(78) Gutiérrez, C. Shining a Light on Chiral Symmetry Breaking in Graphene. *Physics* **2021**, *14*, 76.

(79) Eom, D.; Koo, J.-Y. Direct Measurement of Strain-Driven Kekulé Distortion in Graphene and Its Electronic Properties. *Nanoscale* **2020**, *12* (38), 19604−19608.

(80) Gomes, K. K.; Mar, W.; Ko, W.; Guinea, F.; Manoharan, H. C. Designer Dirac Fermions and Topological Phases in Molecular Graphene. *Nature* **2012**, *483* (7389), 306−310.

(81) Nomura, K.; Ryu, S.; Lee, D.-H. Field-Induced Kosterlitz-Thouless Transition in the N = 0 Landau Level of Graphene. *Phys. Rev. Lett.* **2009**, *103* (21), No. 216801.

(82) Antsyshkina, A. S.; Porai-Koshits, M. A. Dimere complexes in paramagnetic nickel compounds. The structure of $Nien_2Cl_2$ and $Nien_2Br_2$ crystals. *Dokl. Akad. Nauk SSSR* **1962**, *143* (1), 105−108.

(83) Coste, S. C.; Vlaisavljevich, B.; Freedman, D. E. Magnetic Anisotropy from Main-Group Elements: Halides versus Group 14 Elements. *Inorg. Chem.* **2017**, *56* (14), 8195−8202.

(84) Desrochers, P. J.; Telser, J.; Zvyagin, S. A.; Ozarowski, A.; Krzystek, J.; Vicic, D. A. Electronic Structure of Four-Coordinate C_{3v} Nickel(II) Scorpionate Complexes: Investigation by High-Frequency and -Field Electron Paramagnetic Resonance and Electronic Absorption Spectroscopies. *Inorg. Chem.* **2006**, *45* (22), 8930−8941.

(85) Duboc, C.; Phoeung, T.; Zein, S.; Pécaut, J.; Collomb, M.-N.; Neese, F. Origin of the Zero-Field Splitting in Mononuclear Octahedral Dihalide Mn^{II} Complexes: An Investigation by Multi-frequency High-Field Electron Paramagnetic Resonance and Density Functional Theory. *Inorg. Chem.* **2007**, *46* (12), 4905−4916.

(86) Mantel, C.; Baffert, C.; Romero, I.; Deronzier, A.; Pécaut, J.; Collomb, M.-N.; Duboc, C. Structural Characterization and Electronic Properties Determination by High-Field and High-Frequency EPR of a Series of Five-Coordinated Mn(II) Complexes. *Inorg. Chem.* **2004**, *43* (20), 6455−6463.

(87) Kahn, O. *Molecular Magnetism*; VCH: New York, NY, 1993.

(88) Moriya, T. Anisotropic Superexchange Interaction and Weak Ferromagnetism. *Phys. Rev.* **1960**, *120* (1), 91−98.

(89) Dzyaloshinsky, I. A Thermodynamic Theory of "Weak" Ferromagnetism of Antiferromagnetics. *J. Phys. Chem. Solids* **1958**, *4* (4), 241−255.

(90) Coey, M. *Handbook of Magnetism and Magnetic Materials*; Springer: Cham, 2020.

(91) Ketkaew, R.; Tantirungrotechai, Y.; Harding, P.; Chastanet, G.; Guionneau, P.; Marchivie, M.; Harding, D. J. OctaDist: A Tool for Calculating Distortion Parameters in Spin Crossover and Coordination Complexes. *Dalton Trans.* **2021**, *50* (3), 1086−1096.

(92) Liu, X.-T.; Wang, X.-Y.; Zhang, W.-X.; Cui, P.; Gao, S. Weak Ferromagnetism and Dynamic Magnetic Behavior in a Single End-to-End Azide-Bridged Nickel(II) Chain. *Adv. Mater.* **2006**, *18* (21), 2852−2856.

(93) Cao, D.-K.; Li, Y.-Z.; Zheng, L.-M. Layered Cobalt(II) and Nickel(II) Diphosphonates Showing Canted Antiferromagnetism and Slow Relaxation Behavior. *Inorg. Chem.* **2007**, *46* (18), 7571−7578.

(94) Huang, F.-P.; Tian, J.-L.; Li, D.-D.; Chen, G.-J.; Gu, W.; Yan, S.-P.; Liu, X.; Liao, D.-Z.; Cheng, P. Spin Canting and Slow Relaxation in a 3D Pillared Nickel−Organic Framework. *Inorg. Chem.* **2010**, *49* (5), 2525−2529.

(95) Mydosh, J. A. *Spin Glasses: An Experimental Introduction*, 1st ed.; Taylor & Francis Inc.: Bristol, PA, 1993.

(96) Mydosh, J. A. Spin Glasses: Redux: An Updated Experimental/Materials Survey. *Rep. Prog. Phys.* **2015**, *78* (5), No. 052501.

(97) Tholence, J. L. On the Frequency Dependence of the Transition Temperature in Spin Glasses. *Solid State Commun.* **1980**, *35* (2), 113−117.

(98) Mydosh, J. A. Spin-Glasses. *Europhys. News* **1983**, *14* (12), 2−4.

(99) Vincent, E.; Dupuis, V. Spin Glasses: Experimental Signatures and Salient Outcomes. In *Frustrated Materials and Ferroic Glasses*; Lookman, T.; Ren, X., Eds.; Springer International Publishing: Cham, 2018; Vol. *275*, pp 31−56.

(100) Sherrington, D. Materials Physics and Spin Glasses. *J. Phys. A: Math. Theor.* **2019**, *52* (26), No. 264001.

(101) Samarakoon, A.; Sato, T. J.; Chen, T.; Chern, G.-W.; Yang, J.; Klich, I.; Sinclair, R.; Zhou, H.; Lee, S.-H. Aging, Memory, and Nonhierarchical Energy Landscape of Spin Jam. *Proc. Natl. Acad. Sci. U.S.A.* **2016**, *113* (42), 11806−11810.

(102) Khan, N.; Mandal, P.; Prabhakaran, D. Memory Effects and Magnetic Relaxation in Single-Crystalline $La_{0.9}Sr_{0.1}CoO_3$. *Phys. Rev. B* **2014**, *90* (2), No. 024421.

(103) Pazmandi, F.; Domanski, Z. Phase Diagrams of Quantum Spin Glass Models. *J. Phys.: Condens. Matter* **1993**, *5* (9), L117−L122.

(104) Samarakoon, A. M.; Takahashi, M.; Zhang, D.; Yang, J.; Katayama, N.; Sinclair, R.; Zhou, H. D.; Diallo, S. O.; Ehlers, G.; Tennant, D. A.; Wakimoto, S.; Yamada, K.; Chern, G.-W.; Sato, T. J.; Lee, S.-H. Scaling of Memories and Crossover in Glassy Magnets. *Sci. Rep.* **2017**, *7* (1), No. 12053.

(105) Yang, J.; Samarakoon, A.; Dissanayake, S.; Ueda, H.; Klich, I.; Iida, K.; Pajerowski, D.; Butch, N. P.; Huang, Q.; Copley, J. R. D.; Lee, S.-H. Spin Jam Induced by Quantum Fluctuations in a Frustrated Magnet. *Proc. Natl. Acad. Sci. U.S.A.* **2015**, *112* (37), 11519−11523.

(106) Piyakulworawat, C.; Thennakoon, A.; Yang, J.; Yoshizawa, H.; Ueta, D.; Sato, T. J.; Sheng, K.; Chen, W.-T.; Pai, W.-W.; Chou, F.-C.; Matan, K.; Lee, S.-H. Zero-Point Entropies of Spin-Jam and Spin-Glass States in a Frustrated Magnet. *Phys. Rev. B* **2024**, *109*, No. 104420, DOI: 10.1103/PhysRevB.109.104420.

(107) Jonason, K.; Vincent, E.; Hammann, J.; Bouchaud, J. P.; Nordblad, P. Memory and Chaos Effects in Spin Glasses. *Phys. Rev. Lett.* **1998**, *81* (15), 3243−3246.

(108) *Ageing and the Glass Transition*; Henkel, M.; Pleimling, M.; Sanctuary, R., Eds.; Springer: Berlin, 2007.

(109) Baity-Jesi, M.; Calore, E.; Cruz, A.; Fernandez, L. A.; Gil-Narvion, J. M.; Gonzalez-Adalid Pemartin, I.; Gordillo-Guerrero, A.; Iñiguez, D.; Maiorano, A.; Marinari, E.; Martin-Mayor, V.; Moreno-Gordo, J.; Muñoz Sudupe, A.; Navarro, D.; Paga, I.; Parisi, G.; Perez-Gaviro, S.; Ricci-Tersenghi, F.; Ruiz-Lorenzo, J. J.; Schifano, S. F.; Seoane, B.; Tarancon, A.; Yllanes, D. Memory and Rejuvenation Effects in Spin Glasses Are Governed by More than One Length Scale. *Nat. Phys.* **2023**, *19* (7), 978−985.

(110) Lundgren, L.; Svedlindh, P.; Beckman, O. Anomalous Time Dependence of the Susceptibility in a Cu(Mn) Spin Glass. *J. Magn. Magn. Mater.* **1983**, *31*−*34*, 1349−1350.

(111) Jonsson, T.; Jonason, K.; Jönsson, P.; Nordblad, P. Nonequilibrium Dynamics in a Three-Dimensional Spin Glass. *Phys. Rev. B* **1999**, *59* (13), 8770−8777.

(112) Hammann, J.; Vincent, E.; Dupuis, V.; Alba, M.; Ocio, M.; Bouchaud, J.-P. Comparative Review of Aging Properties in Spin Glasses and Other Disordered Materials. *J. Phys. Soc. Jpn.* **2000**, *1*, 206−211.

(113) Bhatti, S.; Sbiaa, R.; Hirohata, A.; Ohno, H.; Fukami, S.; Piramanayagam, S. N. Spintronics Based Random Access Memory: A Review. *Mater. Today* **2017**, *20* (9), 530−548.

(114) De, D.; Goswami, S.; Chakraborty, M. Magnetic Memory Effect: Unfolding Magnetic Metastabilities. *J. Magn. Magn. Mater.* **2023**, *565*, No. 170175.

(115) Wen, J.; Yu, S.-L.; Li, S.; Yu, W.; Li, J.-X. Experimental Identification of Quantum Spin Liquids. *npj Quantum Mater.* **2019**, *4* (1), 12.

(116) Mörée, G.; Leijon, M. Review of Hysteresis Models for Magnetic Materials. *Energies* **2023**, *16* (9), 3908.

(117) Apalkov, D.; Dieny, B.; Slaughter, J. M. Magnetoresistive Random Access Memory. *Proc. IEEE* **2016**, *104* (10), 1796−1830.

(118) Huang, L.; Yu, B.; Zhai, W.; Cui, X.; Zhou, G.; Zhang, J.; Tang, Y.; Zheng, S.; Lin, L.; Yan, Z.; Liu, J.-M. Giant Exchange Bias Induced by Spin-Glass and Antiferromagnetic Coupling in $Fe_{2-x}Ga_xTeO_6$ Single Crystals. *Appl. Phys. Lett.* **2024**, *124* (23), No. 232404.

(119) Grohol, D.; Matan, K.; Cho, J.-H.; Lee, S.-H.; Lynn, J. W.; Nocera, D. G.; Lee, Y. S. Spin Chirality on a Two-Dimensional Frustrated Lattice. *Nat. Mater.* **2005**, *4* (4), 323−328.

(120) Elhajal, M.; Canals, B.; Lacroix, C. Symmetry Breaking Due to Dzyaloshinsky-Moriya Interactions in the Kagomé Lattice. *Phys. Rev. B* **2002**, *66* (1), No. 014422.

(121) Ritchey, I.; Chandra, P.; Coleman, P. Spin Folding in the Two-Dimensional Heisenberg *Kagomé* Antiferromagnet. *Phys. Rev. B* **1993**, *47* (22), 15342−15345.

(122) Kawamura, H. Chiral Ordering in Heisenberg Spin Glasses in Two and Three Dimensions. *Phys. Rev. Lett.* **1992**, *68* (25), 3785−3788.

(123) Maniv, E.; Murphy, R. A.; Haley, S. C.; Doyle, S.; John, C.; Maniv, A.; Ramakrishna, S. K.; Tang, Y.-L.; Ercius, P.; Ramesh, R.; Reyes, A. P.; Long, J. R.; Analytis, J. G. Exchange Bias Due to Coupling between Coexisting Antiferromagnetic and Spin-Glass Orders. *Nat. Phys.* **2021**, *17* (4), 525−530.

(124) Chandra, P.; Coleman, P.; Ritchey, I. The Anisotropic Kagome Antiferromagnet: A Topological Spin Glass? *J. Phys. I France* **1993**, *3* (2), 591−610.

(125) Skumryev, V.; Stoyanov, S.; Zhang, Y.; Hadjipanayis, G.; Givord, D.; Nogués, J. Beating the Superparamagnetic Limit with Exchange Bias. *Nature* **2003**, *423* (6942), 850−853.

(126) Ghosh, M. P.; Kinra, S.; Dagur, D.; Choubey, R. K.; Mukherjee, S. Evidence of Large Exchange Bias Effect in Single-Phase Spinel Ferrite Nanoparticles. *Phys. Scr.* **2020**, *95* (9), No. 095812.

(127) Huang, F.; Xu, X.; Lu, X.; Zhou, M.; Sang, H.; Zhu, J. The Exchange Bias Behavior of $BiFeO_3$ Nanoparticles with Natural Core-Shell Structure. *Sci. Rep.* **2018**, *8* (1), No. 2311.

(128) Ma, J.; Kamiya, Y.; Hong, T.; Cao, H. B.; Ehlers, G.; Tian, W.; Batista, C. D.; Dun, Z. L.; Zhou, H. D.; Matsuda, M. Static and Dynamical Properties of the Spin-1/2 Equilateral Triangular-Lattice Antiferromagnet $Ba_3CoSb_2O_9$. *Phys. Rev. Lett.* **2016**, *116* (8), No. 087201.

(129) Millonas, M. *Fluctuations and Order: The New Synthesis*; Springer US: New York, NY, 1996.

(130) Iida, K.; Yoshida, H. K.; Nakao, A.; Jeschke, H. O.; Iqbal, Y.; Nakajima, K.; Ohira-Kawamura, S.; Munakata, K.; Inamura, Y.; Murai, N.; Ishikado, M.; Kumai, R.; Okada, T.; Oda, M.; Kakurai, K.; Matsuda, M. Q = 0 Long-Range Magnetic Order in Centennialite $CaCu_3(OD)_6Cl_2{\cdot}0.6D_2O$: A Spin-1/2 Perfect Kagome Antiferromagnet with J_1−J_2−J_d. *Phys. Rev. B* **2020**, *101* (22), No. 220408.

(131) Swendsen, R. H.; Wang, J.-S. Replica Monte Carlo Simulation of Spin-Glasses. *Phys. Rev. Lett.* **1986**, *57* (21), 2607−2609.

(132) Katzgraber, H. G.; Palassini, M.; Young, A. P. Monte Carlo Simulations of Spin Glasses at Low Temperatures. *Phys. Rev. B* **2001**, *63* (18), No. 184422.

(133) Metropolis, N.; Rosenbluth, A. W.; Rosenbluth, M. N.; Teller, A. H.; Teller, E. Equation of State Calculations by Fast Computing Machines. *J. Chem. Phys.* **1953**, *21* (6), 1087−1092.

(134) Alcón, I.; Ribas-Ariño, J.; Moreira, I. D. P. R.; Bromley, S. T. Emergent Spin Frustration in Neutral Mixed-Valence 2D Conjugated Polymers: A Potential Quantum Materials Platform. *J. Am. Chem. Soc.* **2023**, *145* (10), 5674−5683.

(135) Kundu, S.; Dey, T.; Mahajan, A. V.; Büttgen, N. $LiZn_2V_3O_8$: A New Geometrically Frustrated Cluster Spin-Glass. *J. Phys.: Condens. Matter* **2020**, *32* (11), No. 115601.

https://doi.org/10.1021/jacs.4c10113
J. Am. Chem. Soc. XXXX, XXX, XXX−XXX